

# Disk Galaxy Evolution Along the Hubble Sequence

Marios Kampakoglou and Joseph Silk

*Department of Physics, University of Oxford, Keble Road, Oxford OX1 3RH, United Kingdom (e-mail: mariosk,silk@astro.ox.ac.uk)*

18 April 2018

## ABSTRACT

Galaxy disks are characterised by star formation histories that vary systematically along the Hubble sequence. We study global star formation, incorporating supernova feedback, gas accretion and enriched outflows in disks modelled by a multiphase interstellar medium in a fixed gravitational potential. The star formation histories, gas distributions and chemical evolution can be explained in a simple sequence of models which are primarily regulated by the cold gas accretion history.

## 1 INTRODUCTION

The two most striking characteristics that define the Hubble sequence are morphology and star formation activity. The former is best addressed by numerical simulations (Abadi et al. (2003); Sharma & Steinmetz (2005); Robertson et al. (2004); Governato et al. (2006)). However the latter aspects are so complex that most discussions of disk star formation and chemical evolution are based on analytical calculations (Efstathiou (2000); Silk (2001); Ferreras & Silk (2001); Silk (2003); Matteucci (2006); Naab & Ostriker (2006)). This paper extends the analytic approach to study star formation histories that vary systematically along the Hubble sequence. We study global star formation, incorporating supernova feedback, gas accretion and enriched outflows in disks modelled by a multi-phase interstellar medium in a fixed gravitational potential.

One of the current problems afflicting galaxy formation models is the role of gas infall. For both ellipticals (Bower et al. (2006); Croton et al. (2006)) and massive disks at  $z \sim 2$  (Forster Schreiber et al. (2006)), infall rates are sufficiently high from CDM theory (ellipticals and disks) and observations (disks) that infall must be quenched, otherwise distant ellipticals are too blue and the disks are too massive by the current epoch. The problems may be related via feedback from AGN, but the details are poorly understood with regard to the resulting star formation history, gas infall rates and chemical evolution. In this paper, we focus on disk galaxies, and develop a phenomenological description of disk evolution in which the onset and duration of the gas infall history are found to be the controlling parameters. The star formation histories, gas distributions and chemical evolution can be explained in a simple sequence of models which are primarily regulated by the cold gas accretion history.

One of the main features of galaxies that characterises the significance of the Hubble sequence is the wide range in young stellar content and star formation activity. This variation in stellar content is part of the basis of the Hubble classification itself, and understanding its physical nature and origins is fundamental to understanding galaxy evolution in its broader context. In this paper, we construct a

sequence of evolutionary models in which present-day properties of different types of disk galaxies are reproduced.

The first implementation of supernova-driven feedback in the context of CDM was to account for the properties of dwarf galaxies (Dekel & Silk (1986)), and subsequent studies have explored the role of supernova feedback in more massive galaxies. Feedback is an important element in our attempts to model galaxy evolution. Energy injection from supernovae is probably the most plausible feedback mechanism for systems with virial temperatures higher than  $10^5$  K. Winds from quasars might also disrupt galaxy formation or limit the growth of central black holes. Here, we will be concerned exclusively with supernova-driven feedback and we will not consider feedback from an active nucleus. The model presented in this paper is similar to the simple self-regulating model with inflow and outflow developed in Efstathiou (2000), the main difference being in the infall model that we implement. We adopt an exponentially decreasing infall rate normalised in order to reproduce the observed total disk mass density in the solar neighbourhood, whereas in Efstathiou’s model it is the conservation of specific angular momentum that specifies the final radius in the disc for each gas element. Angular momentum conservation is known to be a poor approximation, at least in the numerical simulations, and our more phenomenological model is easily adapted to the chemical evolution constraints.

The main result of this paper is that star formation histories of the different types of disk galaxies can be reproduced using a one parameter model. The key parameter of our model is the time corresponding to the onset of the infall. Using this free parameter, we reproduce the distribution of disk birthrate parameters  $b$ , the ratio of the current SFR to the average past SFR, for each type of disk galaxy as presented in Kennicutt et al. (1994) and summarised in Figure 1. We then explore the various implications of the model for the radial and temporal dependences of the gas fraction, star formation rate and metallicity.

The layout of this paper is as follows. Section 2 briefly reviews the main points of our model and presents some basic results. The model is extended in Section 3 to include

arXiv:astro-ph/0610607v2 13 Mar 2007

an improved treatment of winds and chemical evolution. Finally, in Section 4 we discuss our results and present our conclusions.

## 2 MODEL

The model described here is a self-regulating model with inflow and outflow. The disk is considered to be a system of independent rings each of  $35 \times r_d$  pc wide (where  $r_d$  is in units of kpc)<sup>1</sup>. Neither radial inflows nor radial outflows are considered. The ring centred at the galactocentric distance  $r_\odot = 8.5$  kpc is labelled as the solar neighbourhood. For the present-day total disk surface density in the solar neighbourhood, we adopt a value  $\Sigma_{tot}(r_\odot, t_g) = 60 \text{ M}_\odot \text{pc}^{-2}$  (Holmberg & Flynn (2004) found  $56 \pm 6 \text{ M}_\odot \text{pc}^{-2}$  for their disk model).

### 2.1 Dark Halo and Disk Model

The dark halo is assumed to be described by the Navarro, Frenk & White (1995) profile,

$$\rho(r) = \frac{\delta\rho_c}{(Cx)(1+Cx)^2}, \quad (1)$$

where  $x \equiv r/r_v$ ,  $\rho_c$  is the critical density,  $r_v$  is the virial radius at which the halo has mean overdensity of 200 with respect to the background and  $C$  is the concentration parameter. For the present model, we adopt a value for  $C$  of 10. The circular speed corresponding to this profile is

$$v_H^2(r) = v_v^2 \frac{1}{x} \frac{[\ln(1+Cx) - Cx/(1+Cx)]}{[\ln(1+C) - C/(1+C)]}, \quad (2)$$

where  $v_v^2 \equiv \frac{GM_v}{r_v}$ , and  $M_v$  is the mass of the halo within the virial radius.

For the surface density of the disk at  $t = 0$ , we assume an exponential profile:

$$\Sigma_{tot}(r, 0) = \Sigma_0 e^{-\frac{r}{r_d}}, \quad (3)$$

where  $M_D = 2\pi r_d^2 \Sigma_0$ ,  $\Sigma_{tot}(r, 0)$  is the total surface density of the ring centred at galactocentric radius  $r$  at  $t = 0$ ,  $M_D$  is the total disk mass at  $t = 0$  and  $r_d$  is the scale length. So in our model the entire gas disk has formed instantaneously at  $t = 0$ . The rotation curve of a cold exponential disk is given by (Freeman (1970)):

$$v_D^2(r) = 2v_c^2 y^2 [I_0(y)K_0(y) - I_1(y)K_1(y)] \quad (4)$$

where  $y \equiv \frac{r}{2r_d}$  and  $v_c^2 \equiv \frac{GM_D}{r_d}$ . For ratio  $\frac{v_v}{v_c}$  we adopt a value equal to 0.45 that corresponds to the Milky Way. Models using standard disk formation theory with adiabatic contraction within the cuspy halo (Klypin et al. 2002) reproduce the broad range of observational data available for the Milky Way by adopting a virial mass equal to  $M_v \approx 10^{12} \text{ M}_\odot$ , baryonic mass equal to  $M_{bar} \approx 4 - 6 \times 10^{10} \text{ M}_\odot$  and virial radius  $r_v = 258$  kpc. These values in combination with an adopted value for the disk scale length equal to  $r_d = 3$  kpc (Sackett (1997)) give  $\frac{v_v}{v_c} = 0.45$ . In this work, we keep the ratio

$\frac{v_v}{v_c}$  constant for all the models we present.<sup>2</sup> The ratio of virial radius of the halo to disk scale length is defined as the collapse factor  $f_{coll} \equiv \frac{r_v}{r_d} = 50$ ; such a value is needed to reproduce a median value of  $\approx 0.05$  for the dimensionless spin parameter of the halo  $\lambda_H$  (Efstathiou (2000)). The disk is truncated at radius  $r/r_d \approx 7$ .

#### 2.1.1 Two-component(stellar and gas) rotating disk

The stellar radial velocity dispersion  $\sigma_*$  is related to that of the gas clouds:

$$\sigma_* = \alpha \sigma_g, \quad (5)$$

Here we assume  $\alpha = 5$  (Efstathiou (2000)). The scale-height for a two-component rotating disk is (Talbot & Arnett (1975)):

$$H = \frac{\sigma_g^2}{\pi G \Sigma_g} \frac{1}{(1 + \frac{\Sigma_* / \Sigma_g}{\sigma_* / \sigma_g})} \quad (6)$$

### 2.2 Epicyclic frequency Model

The epicyclic frequency is given by the expression

$$\kappa = 2\omega \left(1 + \frac{1}{2} \frac{r}{\omega} \frac{d\omega}{dr}\right)^{1/2}, \quad (7)$$

in which  $\omega$  is the angular velocity of the disk. In the above equation we replace  $\omega = v_{tot}/r$  where  $v_{tot}^2 = v_H^2 + v_D^2$ . So the epicyclic frequency (in units of  $10^{-15} \text{ sec}^{-1}$ ) is:

$$\kappa = 0.035 \sqrt{2} \frac{v_{tot}}{r} \left(1 + \frac{r}{v_{tot}} \frac{dv_{tot}}{dr}\right)^{1/2} \quad (8)$$

### 2.3 Star Formation Rate(SFR)

In this work we adopt the star formation law proposed in Wang & Silk (1994), to which we refer for a detailed description. The star formation rate (in units of  $\text{M}_\odot \text{pc}^{-2} \text{Gyr}^{-1}$ ) is given by :

$$\psi(r, t) = \frac{\epsilon \kappa \Sigma_g (1 - Q^2)^{1/2}}{Q} \quad (9)$$

where  $\kappa$  is the epicyclic frequency,  $\Sigma_g$  is the gas surface density in units of  $\text{M}_\odot \text{pc}^{-2}$ ,  $Q$  is the gravitational instability parameter (Toomre (1964)) and  $\epsilon$  is the efficiency of star formation. For the model in this paper we set  $\epsilon = 0.02$ .

The star formation rate defined above has the following features: (i) star formation can only occur if the disk is gravitationally unstable,  $Q < 1$ ; (ii) the degree of instability of the disk, measured by  $Q$ , is directly linked to the star-formation rate; the smaller  $Q$  is, the more rapidly stars are formed.

The stability criterion for a two-component (stellar and gas) rotating disk can be written as (Wang & Silk (1994)):

$$Q = \frac{\kappa}{\pi G} \left( \frac{\Sigma_g}{\sigma_g} + \frac{\Sigma_*}{\sigma_*} \right)^{-1} \quad (10)$$

<sup>2</sup> The ratio  $\frac{v_v}{v_c}$  defines the disk scale length  $r_d$ . The disk scale length is  $r_d = \frac{(3M_D / (4\pi 200\rho_c f_{coll} (\frac{v_v}{v_c})^2))^{1/3}}{f_{coll}}$  kpc

<sup>1</sup> For a disk galaxy with scale length  $r_d = 3$  kpc the width of each zone is equal to  $35 \times 3 = 105$  pc

where  $\Sigma_*$  and  $\sigma_*$  are the stellar surface density (in units of  $M_\odot \text{pc}^{-2}$ ) and the radial velocity dispersion (in units of  $\text{km sec}^{-1}$ ), and  $\kappa$  is the epicyclic frequency.

## 2.4 IMF

The adopted stellar initial mass function is of the standard Salpeter form :

$$\frac{dN_\star}{dm} = Bm^{-(1+x)}, \quad m_l < m < m_u, \quad x = 1.35 \quad (11)$$

where  $m_l = 0.1 M_\odot, m_u = 50M_\odot$ .

For the IMF adopted, one supernova is formed for every  $125M_\odot$  of star formation, assuming that each star of mass greater than  $8M_\odot$  releases  $10^{51} E_{51}$  ergs in kinetic energy in a supernova explosion. Therefore, the energy injection rate per unit surface area (in units of  $\text{erg s}^{-1} \text{pc}^{-2}$ ) is given by:

$$\dot{E}_{sn}^\Omega = 2.5 \times 10^{32} E_{51} \epsilon_c \psi \quad (12)$$

where the parameter  $\epsilon_c$  defines the percentage of supernovae energy that goes to the ambient medium. For this model we adopt  $\epsilon_c = 0.03$ .

## 2.5 Energy dissipation due to cloud inelastic collisions

The rate of energy loss per unit surface area (in units of  $\text{ergs}^{-1} \text{pc}^{-2}$ ) is given by (Efstathiou (2000)):

$$\dot{E}_{coll}^\Omega = 5 \times 10^{29} \left(1 + \frac{\Sigma_\star / \Sigma_g}{\sigma_\star / \sigma_g}\right) \sigma_{5g} \Sigma_{5g}^3. \quad (13)$$

Using the above equations we know the energy balance in each ring of the disk. We define the radial velocity dispersion of clouds (in units of  $\text{kms}^{-1}$ ) as:

$$\sigma_g(r, t) = \sqrt{\frac{2 \times E(r, t)}{M_g(r, t)}} \quad (14)$$

where  $E(r, t)$  is the energy balance at galactocentric radius  $r$  and time  $t$ , and  $M_g(r, t)$  is the mass of the cold gas at galactocentric radius  $r$  and time  $t$ .

In summary, the energy balance in each ring of the disk defines the cloud and stellar radial velocity dispersion  $\sigma_g, \sigma_*$  through equation (14) and equation (5). Combining this piece of information with the cloud and stellar surface densities  $\Sigma_g, \Sigma_*$ , we calculate the degree of instability at galactocentric radius  $r$  through equation(10). The star formation rate is regulated by the degree of instability, so the final form of the star formation rate is derived by inserting equation (10) into equation (9).

## 2.6 Infall Model

The adopted form for the gas infall rate is an exponentially decreasing function in which the rate of gas infall (in units of  $M_\odot \text{pc}^{-2} \text{Gyr}^{-1}$ ) in each ring is expressed as:

$$f(r, t) = A(r) e^{-\frac{t}{\tau_f}} \quad (15)$$

where  $\tau_f$  (in units of Gyr) is the infall time scale. The infall rate  $f(r, t)$  is normalised to the present-day local disk density,  $\int_{t_{low}}^{t_g} f(r, t) dt = \Sigma_{tot}(r, t_g)$ , where  $\Sigma_{tot}(r, t_g)$  is the present-day total disk surface density of the ring centred at

galactocentric radius  $r$ , and  $t_g$  is the age of the galactic disk ( $t_g = 10$  Gyr). Assuming that the present-day total masses of the different rings exponentially decrease with increasing galactocentric distance with scale-length  $r_d$ , the form of  $A(r)$  can be written as (Chang et al. (2002)):

$$A(r) = \frac{\Sigma_{tot}(r_\odot, t_g) - \Sigma_{tot}(r_\odot, 0)}{\int_{t_{low}}^{t_g} e^{-\frac{t}{\tau_f}} dt} e^{-\frac{(r-r_\odot)}{r_d}} \quad (16)$$

where  $\Sigma_{tot}(r_\odot, 0)$  is the total disk surface density in the solar neighbourhood at the epoch which the formation of the disk begins, and  $\Sigma_{tot}(r_\odot, t_g)$  is the present-day total disk surface density in the solar neighbourhood. We adopt an exponentially decreasing infall rate normalised in order to reproduce the observed total mass density in the solar neighbourhood. In our infall model, we have introduced a parameter  $t_{low}$  that corresponds to the time that infall switches on. Adjusting this parameter we can reproduce the distribution of disk birthrate parameter  $b$ , the ratio of the current SFR to the average past SFR, for each type of galaxy presented in Kennicutt et al. (1994). The infall time scale  $\tau_f$  (in units of Gyr) is also a free parameter of the model but we keep it constant, adopting a value of 0.5 Gyr.

According to the adopted infall form, since  $\tau_f$  does not vary with radius, the disk keeps the exponential form with scale length  $r_d$  at each epoch of evolutionary time.

## 2.7 Hot Phase Model

An expanding supernova remnant will evaporate a mass of cold gas. The rate of the evaporated mass per unit area is (Efstathiou 2000):

$$\dot{M}_{ev}^\Omega \approx 1 \times 10^{-7} \frac{\sigma_{5g}^2}{\Sigma_{5g} \left(1 + \frac{\Sigma_\star / \Sigma_g}{\sigma_\star / \sigma_g}\right)} \times S_{13}^{0.71} \gamma^{0.29} E_{51}^{0.71} f_\Sigma^{-0.29} \quad (17)$$

in units of  $M_\odot \text{pc}^{-2} \text{yr}^{-1}$ , where  $\Sigma_{5g}$  is the gas surface density in units of  $5 M_\odot \text{pc}^{-2}$ ,  $\sigma_{5g}$  is the cloud radial velocity dispersion in units of  $5 \text{kms}^{-1}$  and  $S_{13}$  is the supernovae rate in units of  $10^{-13} \text{pc}^{-3} \text{yr}^{-1}$ . The parameter  $\gamma$  relates the blast wave velocity to the isothermal sound speed ( $v_b = \gamma c_h$ ,  $\gamma \approx 2.5$ ). The parameter  $f_\Sigma$  is defined through the evaporation parameter (in units of  $\text{pc}^2$ ):

$$\Sigma^{ev} = 280 \frac{\sigma_{5g}^2}{\Sigma_{5g}^2} \frac{1}{\left(1 + \frac{\Sigma_\star}{\sigma_\star / \sigma_g}\right)} \frac{1}{\phi_\kappa} = f_\Sigma \Sigma^{ev\odot} \quad (18)$$

where  $\Sigma^{ev\odot}$  is the evaporation parameter in the local solar neighbourhood and  $\phi_\kappa$  is a parameter that quantifies the effectiveness of classical thermal conductivity. For this model we adopt  $\Sigma^{ev\odot} = 95 \text{pc}^2$  and  $\phi_\kappa = 0.1$ . For a system with porosity  $Q$  close to unity, the temperature and the age of a supernovae remnant are given by:

$$t_o = 5.5 \times 10^6 S_{13}^{-5/11} \gamma^{-6/11} E_{51}^{-3/11} n_h^{3/11} \text{yr}, \quad (19)$$

$$T_o = 1.2 \times 10^4 S_{13}^{6/11} \gamma^{-6/11} E_{51}^{8/11} n_h^{-8/11} \text{K}, \quad (20)$$

The density of the ambient hot phase is

$$n_h = 4.3 \times 10^{-3} S_{13}^{0.36} \gamma^{-0.36} E_{51}^{0.61} f_\Sigma^{-0.393} \text{cm}^{-3}. \quad (21)$$

For  $10^5 \leq T \leq 10^6$  K we adopt a cooling rate of  $\Lambda \approx 2.5 \times 10^{-22} T_5^{-1.4} \text{ erg cm}^3 \text{ s}^{-1}$ . So for a gas with primordial composition, the cooling time  $t_{cool}$  is

$$t_{cool} = 2t_o T_5^{2.4} f_{\Sigma}^{0.5} \quad (22)$$

## 2.8 Outflow Model

As mentioned in the previous section, supernova bubbles expand, evaporate cold gas and compress the ambient interstellar medium (ISM). The compressed ISM will also be driven by a form of wind. In order to study the effects of outflow, we assume a simple phenomenological model for galactic winds where the wind mass-loss rate  $\dot{M}_W$  (in units of  $M_{\odot} \text{ pc}^{-2} \text{ Gyr}^{-1}$ ) is assumed to be proportional to the star formation rate.

$$\dot{M}_W = k\psi. \quad (23)$$

We explore many values of  $k$  between 0 and 1. The hot gas that escapes from the halo is removed permanently. Superwinds indeed are found around Milky Way-type galaxies (Strickland et al. 2007). This is puzzling from the theoretical perspective because supernovae are considered to be incapable of driving a strong wind from the gravitational potential well of a massive galaxy. Also, at least one example is known of an extended x-ray halo around a normal massive spiral galaxy (Pedersen et al. 2006). In this case, gravitational accretion and shock heating provides the most plausible source for heating the gas.

## 2.9 Galactic Fountain Model

Models of gas flow on the galactic scale were first introduced by Shapiro & Field (1976) and subsequently developed by Bregman (1980) and others. The galactic fountain originates from the supernovae that warms up the disk gas to temperatures of  $10^6$  K. The upflowing gas cools and condenses into neutral hydrogen clouds that rains onto the disk. The models assume the height to which the hot gas will rise and the expected rate of condensation in the cooling gas depends only on the temperature of the gas at the base of the fountain and the rate of cooling of the upflowing gas. In the model described in this paper the hot gas that is not lost from the disk returns to the disk at the radius from which it was expelled after a time  $t_{cool}$ .

## 2.10 Chemical Evolution

We include chemical evolution in the model using the instantaneous recycling approximation. So we assume that all processes involving stellar evolution, nucleosynthesis and recycling take place instantaneously on the time scale of galactic evolution. The equation of galactic chemical evolution is

$$\Sigma_g dZ = p\psi dt + (Z_F - Z)f \quad (24)$$

where  $f$  is the infall rate (in units of  $M_{\odot} \text{ pc}^{-2} \text{ Gyr}^{-1}$ ) and  $p$  is the yield (Pagel (1997)). We adopt a yield of  $p = 0.02$  and assume that the mass accreted to the disk has zero metallicity ( $Z_F = 0$ ). We normalise the metallicities to the solar value for which we adopt  $Z_{\odot} = 0.02$ .

Input parameters	
Solar radius	$r_{\odot} = 8.5 \text{ kpc}$
Total disk surface density at $r_{\odot}$	$\Sigma_{tot}(r_{\odot}, t_g) = 60 M_{\odot} \text{ pc}^{-2}$
Star Formation IMF	Salpeter
Solar metallicity	$Z_{\odot} = 0.02$
Effective yield	$p = 0.02$
Star formation efficiency	$\epsilon = 0.02$
Infall timescale	$\tau_f = 0.5 \text{ Gyr}$
Galactic disk age	$t_g = 10 \text{ Gyr}$
Thermal Conductivity effectiveness	$\phi_{\kappa} = 0.1$
Solar evaporation parameter	$\Sigma_{\odot}^{ev} = 95 \text{ pc}^2$
Disk to Halo velocity ratio	$\frac{v_w}{v_c} = 0.45$
Collapse factor	$f_{coll} = 50$
Wind Model Parameter	$k = 0.2$

**Table 1.** Input parameters in common for the five models we examine in this paper.

Type	Disk Mass $M_D(M_{\odot})$	$r_d(\text{kpc})$
Sa	$5.5 \times 10^{10}$	3.
Sb	$4. \times 10^{10}$	2.7
Sc	$2.7 \times 10^{10}$	2.37
Sd	$1.5 \times 10^{10}$	1.95
Sm	$1. \times 10^{10}$	1.7

**Table 2.** Five models adopted in this paper

## 2.11 Different Types of Spiral Galaxies

To explore the evolution of different types of spiral galaxies we adopt five models in this paper (See Table 2). These models differ only in the mass of the disk and the disk scale length  $r_d$ . All the input parameters that these models have in common are summarized in Table 1.

## 2.12 Basic Results

In this section will present the basic results of the model discussed in the previous sections. Unless otherwise stated, we adopt a value 0.2 for the parameter  $k$  in the outflow model. For clarification of the plots, when results from models Sc and Sd are similar we define a new type of disk galaxy Sc/d. The data for Sc/d type come from the average between the Sc model data set and the Sd model data set.

### 2.12.1 Distribution of disk birth rate $b$

Values of the birth parameter  $b$  were calculated for each type of spiral galaxy. For the calculation of  $b$  values we ignore the SFR that corresponds to the first  $10^8$  yr, due to a deficiency in our model. More specifically in the model we assume that the entire gas disk has formed instantaneously at  $t = 0$ : this is unrealistic and leads to very high rates of star formation for the first  $10^8$  yr. Figure 2 shows the disk birthrate parameter  $b$  subdivided by galaxy type as a function of our free parameter  $t_{low}$  that corresponds to the time that infall switches on. The dotted line indicates the median value of birthrate parameter while the dashed lines show the quartiles of birthrate parameter presented in Kennicutt et al.

<i>Type</i>	<i>b</i> (median)	$t_{low\_med}$ (Gyr)
Sa	0.07	0.10
Sb	0.37	7.00
Sc	1.04	8.05
Sd	0.63	7.80
Sm	1.31	8.35

**Table 3.** Median value of  $b$  and  $t_{low}$  value for different models.

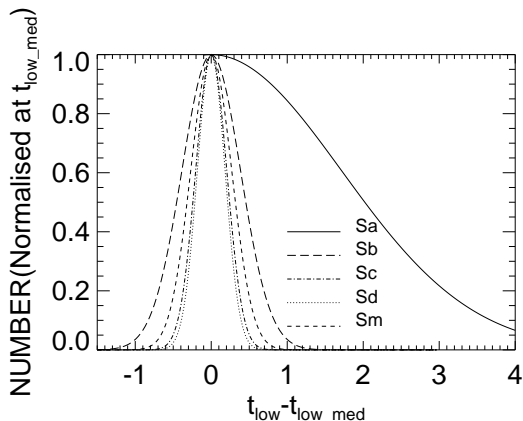


**Figure 1.** Gaussian fits to the  $b$  parameter dispersion for each type of disk galaxy

(1994). In Table 3, we present the value of the free parameter  $t_{low}$  we adopt in order to reproduce the median value of birthrate parameter for each type of disk galaxy.

To make our results more useful for observers, we fit Gaussians to the  $b$  parameter dispersion for each type of disk galaxy (Figure 1). The full width at half maximum for each different Gaussian equals the width of the  $t_{low}$  parameter distribution in order to reproduce the quartiles of the  $b$  parameter distribution presented in Kennicutt et al. (1994). In Table 4, we give the value of  $\sigma$  for the Gaussian fits as well as the width in  $t_{low}$  in order to reproduce the quartiles of the  $b$  parameter distribution. The width of the  $b$  parameter distribution between the quartiles for each type of disk galaxy is presented in the last column.

<i>Type</i>	$\sigma$	$\Delta t_{low}$ (Gyr)	$\Delta b$
Sa	1.716	4.04	0.1
Sb	0.386	0.91	0.3
Sc	0.205	0.48	0.6
Sd	0.183	0.43	0.4
Sm	0.270	0.64	2.0

**Table 4.** The value of  $\sigma$  for the Gaussian fits (second column), the width in  $t_{low}$  in order to reproduce the quartiles of the  $b$  parameter distribution (third column), the width of the  $b$  parameter distribution between the quartiles of the distributions (fourth column). The values are shown for different types of disk galaxies.

### 2.12.2 Density Profiles

Figure 3 and figure 4 show the evolution of the gas and stellar surface densities, respectively, (in units of  $M_{\odot}pc^{-2}$ ) for different ages and different type of disk galaxies. The results are shown for ages of 0, 0.1, 1, 3, 6 (top - bottom) and 10 Gyr (*dashed* line). The star formation rates are initially high and hence the time scale for star formation is short. Almost the total amount of gas in the central region of disk is transformed to stars in  $10^8$ yr. The star formation rate declines rapidly after 1 Gyr. As figure 3 and figure 4 show the star formation at early times is concentrated to the inner parts of the disk which have a high surface density, and hence the gas distribution develops a surface density profile with an inner 'hole', similar to what is seen in the HI distributions in real galaxies (Deul & den Hartog (1990)).

Model Sa has parameters similar to those of the Milky Way. Gas surface densities from direct observations at the solar neighbourhood is  $8 \pm 5 M_{\odot}/pc^2$  (Dame (1993)) in good agreement with the predictions of the model. Slightly higher values of  $\approx 13 - 14 M_{\odot}/pc^2$  have been reported by Olling & Merrifield (2001) and are in good agreement with measurements of Milky Way scalelength ( $r_d \approx 2.5 - 3.5kpc$  Sackett (1997)) Sb model can also be a good candidate for the Milky Way.

Direct observations of the stars at the solar neighbourhood of Milky Way by Gould et al. (1996) and Zheng et al. (2001) using HST observations of M stars in the Galactic disk determine a surface density of  $12.2 - 14.3 M_{\odot}/pc^2$ . Visible stars other than M stars contribute  $\approx 15 M_{\odot}/pc^2$ , resulting in a total stellar surface density in the range of  $\approx 27 - 30 M_{\odot}/pc^2$ . This value is in good agreement with predictions from Sa and Sb models.

### 2.12.3 Gas Velocity Profiles

Figure 5 shows the radial distribution of the gas velocity at 10 Gyr for different types of disk galaxies, Sa (*solid* line), Sb (*thick solid* line), Sc (*dashed* line), Sd (*thick dashed* line) and Sm (*dotted* line). Gas velocity profiles are in good agreement with recent theoretical predictions (Ricotti & Ferrara 2002) that in a multiphase low metallicity ( $Z \approx 5 \times 10^{-3} Z_{\odot}$ ) interstellar medium the velocity probability distribution should be close to a Maxwellian with velocity dispersion  $\sigma \geq 11 km/sec^{-1}$ . Furthermore studies of nearby face-on galaxies show that the velocity dispersion in the HI layer is decreasing monotonically from about  $10 - 13 km s^{-1}$  in the optically bright inner regions to  $6 - 8 km s^{-1}$  in the very outer parts (Kamphuis & Sancisi (1993)).

### 2.12.4 Star formation Profiles

Figure 6 shows the evolution of the radial distribution of the star formation rate for different ages and different types of disk galaxies. The results are shown for ages of 0.1 (*solid* line), 1 (*solid thick* line), 3 (*dashed* line), 6 (*dashed thick* line) and 10 Gyr (*dotted* line).

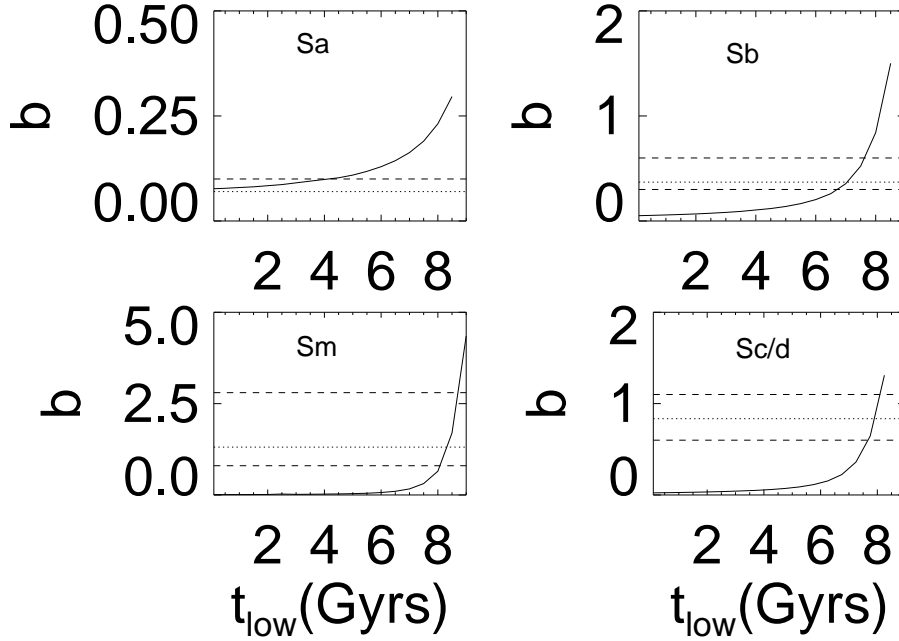


**Figure 2.** The disk birthrate parameter  $b$ , the ratio of current SFR to the average past SFR, plotted against the free parameter  $t_{low}$ , for different types of disk galaxies. The dotted line indicates the median values of birthrate parameter while the dashed lines show the quartiles of birthrate parameter presented by Kennicutt et al. For clarification of the plot, we define a new type of disk galaxy Sc/d. The data for Sc/d type come from the average between the Sc model data set and the Sd model data set.

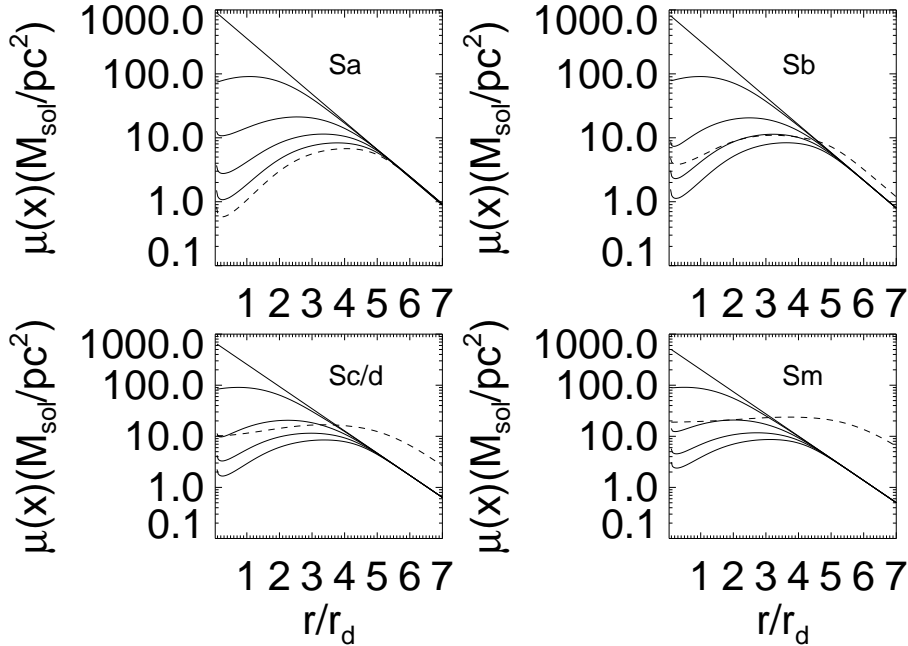


**Figure 3.** The evolution of the gas surface densities for different ages and different types of disk galaxies. The results are shown for ages (top - bottom) of 0, 0.1, 1, 3, 6 and 10 Gyr (*dashed* line).

### 2.12.5 Metallicity Profiles

Figure 7 shows the evolution of the radial distribution of gas metallicity for different ages and different type of disk galaxies. The results are shown for ages of 0.1 (*solid* line) and 10 Gyr (*dotted* line).

Note the very high value of metallicity for Sa type galax-

ies today. The model predicts that metal-rich winds are needed especially for Sa type galaxies in order to produce reasonable values for metallicity today. This prediction is in

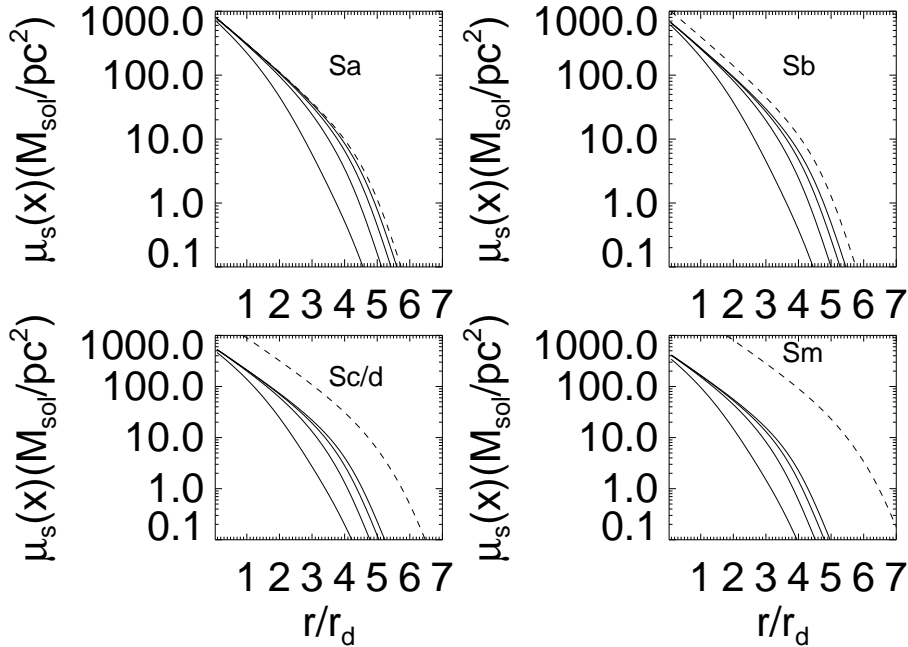


**Figure 4.** The evolution of stellar surface densities for different ages and different types of disk galaxies. The results are shown for ages (top - bottom) of 0, 0.1, 1, 3, 6 and 10 Gyr (*dashed line*).

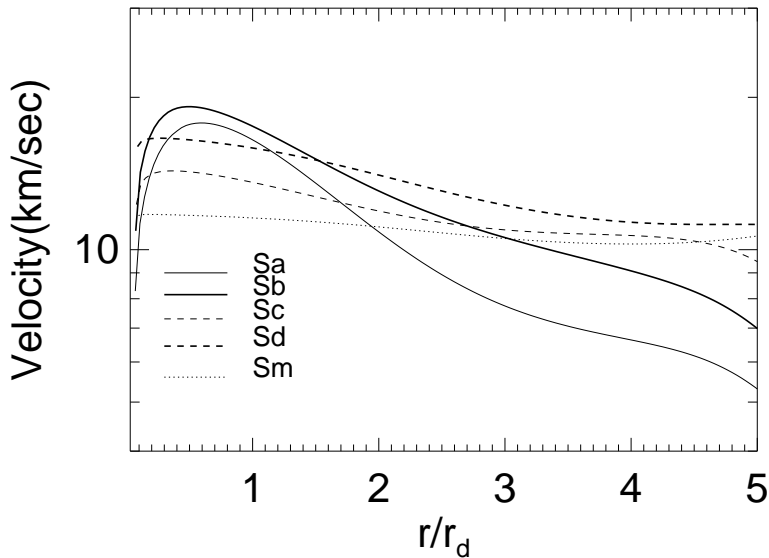


**Figure 5.** The radial distribution of the gas velocity at 10 Gyr for different types of disk galaxies, Sa (*solid line*), Sb (*thick solid line*), Sc (*dashed line*), Sd (*thick dashed line*) and Sm (*dotted line*).

agreement with suggestions presented in Dalcanton (2006) (for more detailed comments see Section 3.2)<sup>3</sup>.

<sup>3</sup> Note that metallicity today does decline slightly close to the center. This is due to the radial profile we choose for the infall rate since we add most of the fresh low metallicity gas to the central regions.

#### 2.12.6 Infall Rate Profiles

The evolution of the radial distribution of the infall rate (in units of  $M_{\odot} \text{pc}^{-2} \text{Gyr}^{-1}$ ) is shown in Figure 8. The results are shown for different ages. As already mentioned the time when the infall switches on is defined by the free parameter  $t_{low}$ . For the results presented in figure 5, we adopt for  $t_{low}$  a value that reproduces the median value of birth parameter  $b$  for each type of disk galaxy. For Sa galaxies the results are

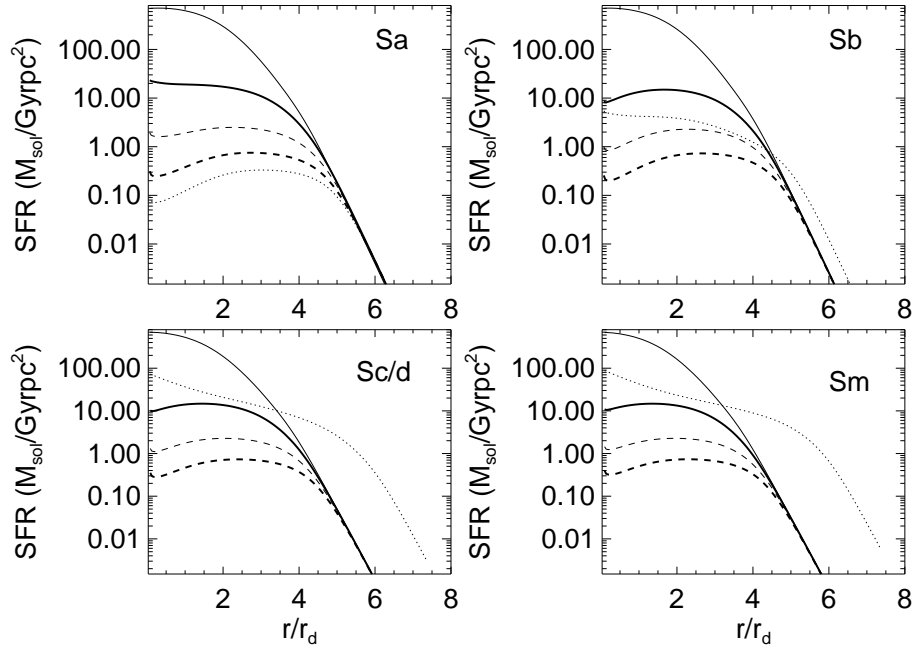


**Figure 6.** The evolution of the radial distribution of the star formation rate for different ages and different types of disk galaxies. The results are shown for ages of 0.1 (*solid line*), 1 (*solid thick line*), 3 (*dashed line*), 6 (*dashed thick line*) and 10 Gyr (*dotted line*).

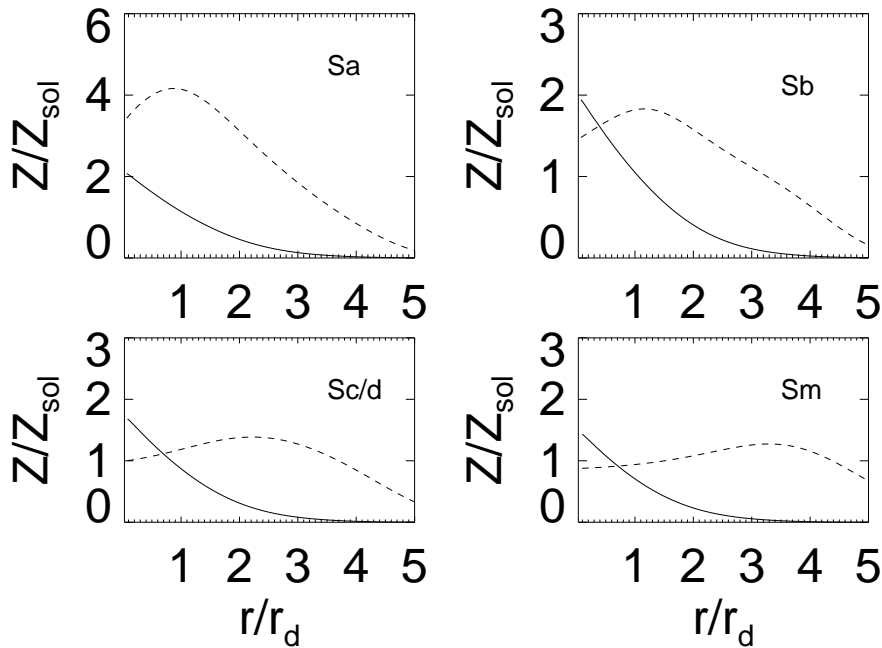


**Figure 7.** The evolution of the radial distribution of gas metallicity for different ages and different types of disk galaxies. The results are shown for ages of 0.1 (*solid line*) and 10 Gyr (*dotted line*).

shown for 3 (*solid line*) and 6 Gyr (*dashed line*). Infall rates for Sb, Sc, Sd, and Sm galaxies are presented for ages of 8.5 (*solid line*) and 10 Gyr (*dashed line*). Note the different range in the y axis for different types of disk galaxies.

### 2.12.7 Disk Global Properties

Figure 9 shows the net star formation rates (upper panel) and the evolution of gas fraction and total disk mass, stars

plus gas (middle panels), for different types of disk galaxies respectively. Note the very high values for the infall rate for the Sb, Sc, Sd and Sm galaxies. Since these galaxies have smaller mass and the infall is switched on much later in comparison with the Sa type, we need high infall rates in order to reproduce the observed total mass density in the solar neighbourhood.



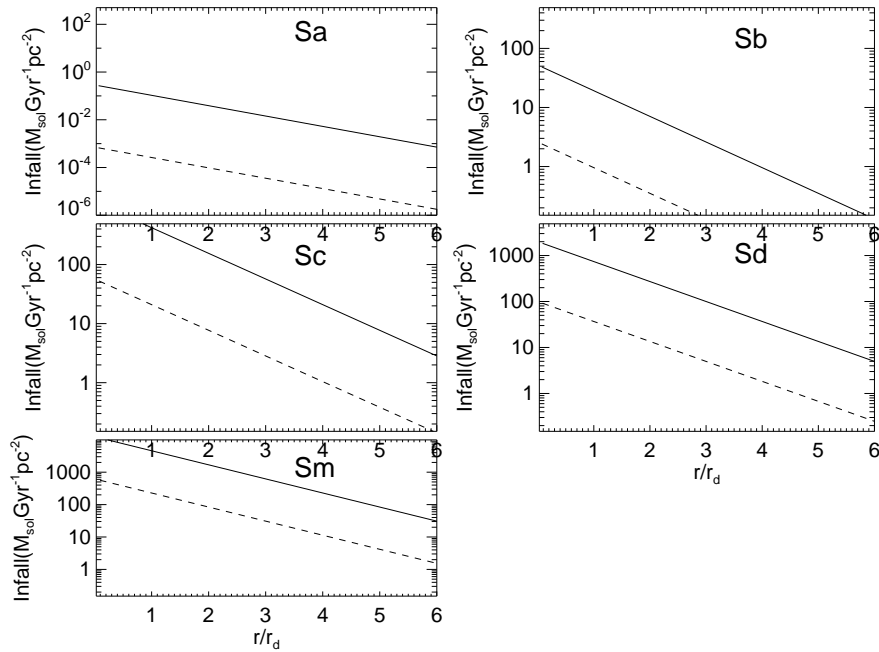


**Figure 8.** The evolution of the radial distribution of the infall rate for different ages and different types of disk galaxies. For Sa galaxies the results are shown for 3 (*solid line*) and 6 Gyr (*dashed line*). Infall rates for Sb, Sc, Sd, and Sm galaxies are presented for ages of 8.5 (*solid line*) and 10 Gyr (*dashed line*)

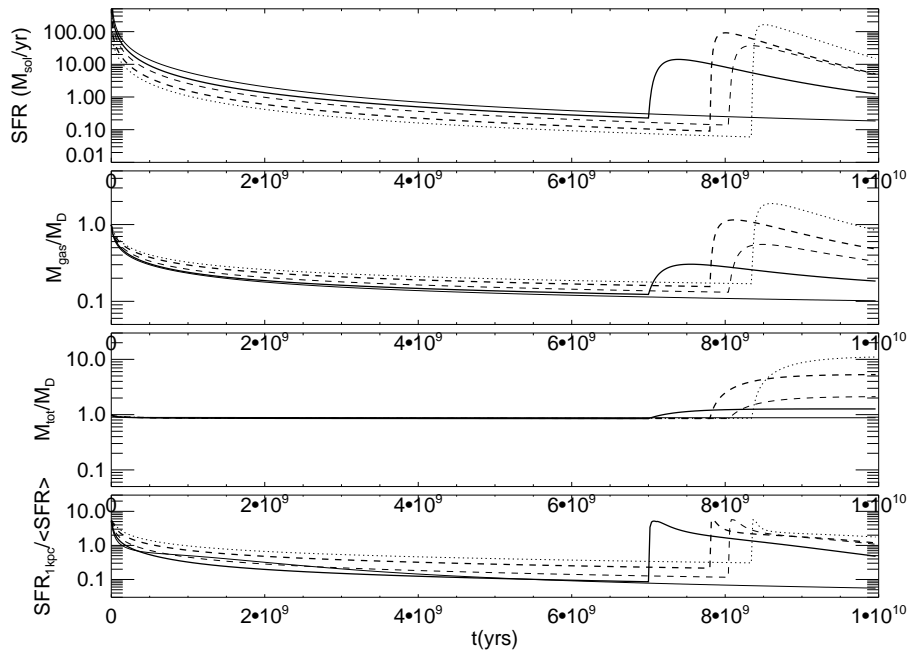


**Figure 9.** Upper panel: time evolution of net star formation rate. Middle panels: time evolution of gas fraction and total disk mass (stars plus gas). Bottom panel: ratio of star formation rate at  $r = 1 \text{ kpc}$  over the mean star formation rate. The results are shown for different types of disk galaxies, Sa (*solid line*), Sb (*solid thick line*), Sc (*dashed line*), Sd (*dashed thick line*) and Sm (*dotted line*).

## 2.13 Star formation rate histories

### 2.13.1 Galactocentric radius $r = 1 \text{ kpc}$

In this section, we present results for the star formation rate history at galactocentric radius  $r = 1 \text{ kpc}$  for different types of disk galaxies.

In figure 9, we show the star formation rate history at galactocentric radius equal to  $r = 1 \text{ kpc}$  (bottom panel) for different types of disk galaxies. Note, that galaxy types which are characterised by large infall rates (Sb, Sc, Sd, Sm) show a peak at the onset of infall. At time  $t = t_{\text{low}}$ , when the infall

de Vaucouleurs	Sa	Sb	Sc	Sd	Sm
T	1	3	5	7	9

**Table 5.** Definition of numerical type  $T$ 

switches on, the accreted gas increases the local star formation rate by a bigger factor in comparison with the increase in the mean star formation rate across the disk and causes the peak in Figure 9. This phenomenon is much stronger at smaller radii because of the inner 'hole' that has developed in the surface density of the gas at late times (see figure 3). At late times, the star formation in the inner parts of the disk is stopped due to lack of gas, but the fresh gas comes in at  $t = t_{low}$  to refuel the central regions and increase the local star formation by a big factor. For Sa galaxies, the infall rate is very small so the curve in figure 9 is smooth.

### 3 REFINEMENTS OF THE MODEL

The model described in the previous section contain a number of simplifications, which we will attempt to refine in this section. We introduce some simple improvements to the outflow model (Section 3.1) and to the chemical evolution model (Section 3.2).

#### 3.1 Outflow model

In Section 2.8 we assumed that the  $k$  parameter is constant. Instead of keeping the  $k$  parameter in the outflow model constant for the different types of disk galaxies, we can assume that  $k$  is proportional to the ratio of bulge-to-disk circular velocities. This is a reasonable assumption especially if we believe that AGN feedback contributes to the wind mechanism. For systems with constant density, the bulge-to-disk velocity ratio can be reduced to the following expression:

$$\frac{v_b}{v_d} \propto \left(\frac{r_e}{r_d}\right)^{1/a} \quad (25)$$

where  $r_e$  is the effective radius of the bulge and  $r_d$  is the the disk scale length. Following MacArthur et al. (2003), we can use the following expression for the  $\frac{r_e}{r_{disk}}$  ratio :

$$\frac{r_e}{r_d} = 0.20 - 0.013(T - 5), \quad (26)$$

where  $T$  defines the galaxy type. The relationship between  $T$  and galaxy type is shown in Table 5. Note that eq. 26 is valid only for galaxies with numerical type  $T$  between 1 and 7. Initial investigation of equation 26, using  $a = 1$  and  $a = 2$ , shows that our results are insensitive to this refinement of the model. We plan to investigate the implications of equation (26) in more detail in a future paper.

#### 3.2 Chemical evolution

In Section 2.10, we assumed that gas ejected from the disk has the same metallicity as the ISM at the time that the gas was ejected. Due to this assumption, the predicted metallicity curve for Sa and Sb galaxies today is very high (see Figure 7, top panel). This problem does not appear in smaller

galaxies (Sc, Sd, Sm) because the infall rate is higher than the rate of star formation, thus allowing the accreted metal-poor gas to dilute the ISM faster than it can be enriched by evolving stars. A comparison with observational data (Pilyugin et al. (2004); Kewley et al. (2005)) leaves metal-rich outflows as the only viable mechanism for producing the low effective yields observed in gas-rich galaxies. Following Dalcanton (2006), we parameterise the metallicity  $Z_{SN}$  of the SN ejecta as a multiple  $\eta$  of the nucleosynthetic yield. For a Salpeter IMF  $\eta = 6.2 - 7.1$ . For this paper, we adopt a value  $\eta = 4.25$  for Sa type galaxies and a smaller value  $\eta = 2$  for the other galaxy types. Furthermore, in this improved model for chemical evolution for the accreted gas, we adopt a metallicity of  $Z_F = 0.1 \times Z_\odot$ . The equation of galactic chemical evolution is :

$$\Sigma_g dZ = p\psi dt + (Z_F - Z)f - Z(\eta - 1)\dot{M}_W \quad (27)$$

In figure 10 we show the evolution of the radial distribution of gas metallicity for different ages and different type of disk galaxies. The results are shown for ages of 0.1 (*solid* line) and 10 Gyr (*dotted* line). Comparison between the model predictions and the observational data is shown in figure 12. The results come from Kewley et al. (2005) (Table 2 in this paper). For the oxygen abundance in the solar neighbourhood, we adopt a value  $12 + 0/H = 8.5$  (Pilyugin et al. (2002)). The model predictions for global metallicities are calculated assuming that the disk is truncated at  $r/r_d \approx 5$ .

Figure 11 shows the radial metallicity distribution of the interstellar medium for each of our disk models after 10 Gyr (*dashed* line). For the Sa model which is similar to the Milky Way the metallicity gradient is about  $d\log(Z)/dr = -0.055 \text{ dexkpc}^{-1}$  at the solar radius. Observational values for the metallicity gradient of light elements X in the Milky Way are in the range of  $-0.04 < d\log(X/H)/dr < -0.08 \text{ dexkpc}^{-1}$  (Chiappini et al. (2001)). Our models predict that the metallicity gradient at the solar radius of the disks depends on the type, and increases as we go from early spirals to later types in agreement with observations (Marquez et al. (2002)). Our predictions for the metallicity gradient of later type disk galaxies are in reasonable agreement with observations (Vila-Costas & Edmunds (1992)) although there is a considerable scatter in the published values.

## 4 DISCUSSION

We have presented a model of global star formation incorporating supernova feedback, gas accretion and enriched outflows in disks modelled by a multiphase interstellar medium in a fixed gravitational potential.

A key prediction of this model is that star formation histories of different types of disk galaxies can be explained in a simple sequence of models which are primarily regulated by the cold gas accretion history. The distributions of disk birth parameters presented in Kennicutt et al. (1994) are reproduced using the parameter  $t_{low}$  which varies with the type of disk galaxy. Sa galaxies are characterised by quiescent evolution and a small value for the  $t_{low}$  parameter whereas Sb, Sc, Sd and Sm galaxies are characterised by starbursts and relatively large values for the  $t_{low}$  parameter.

A description of disk evolution in which the onset and

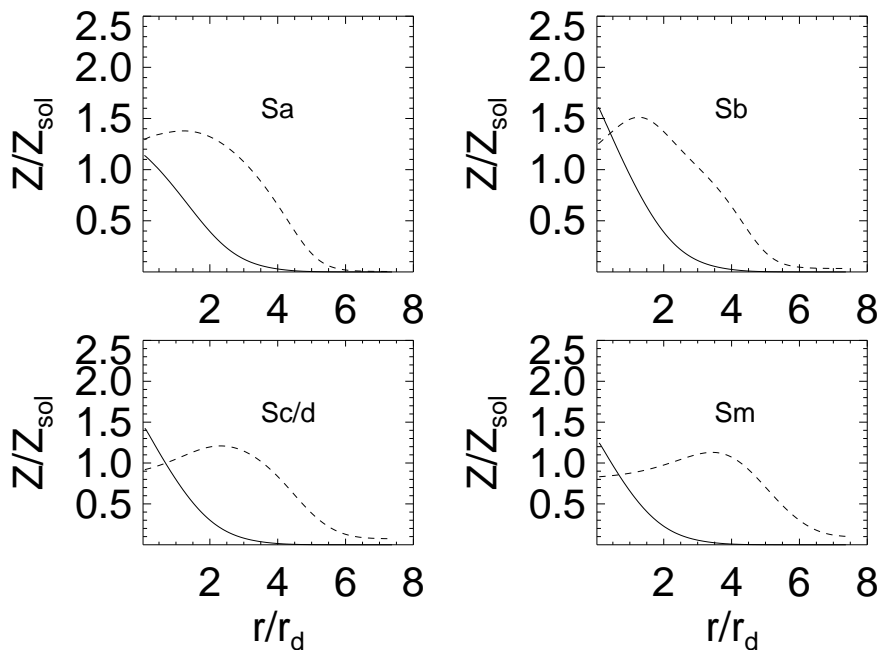


**Figure 10.** The evolution of the radial distribution of metallicity for different ages and different types of disk galaxies. The results are shown for ages of 0.1 (*solid line*) and 10 Gyr (*dashed line*).

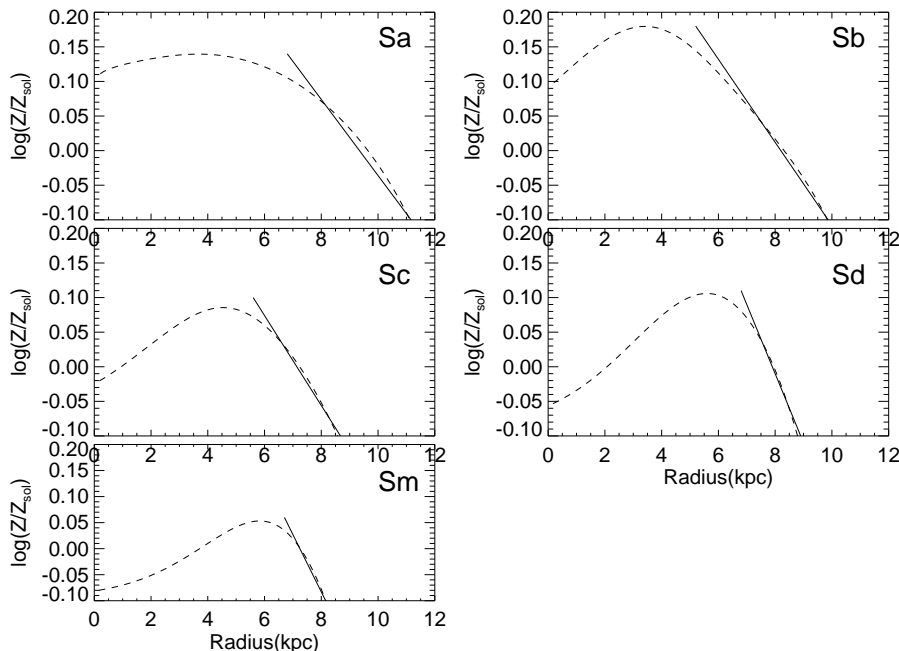


**Figure 11.** Radial metallicity distribution of the gas after 10 Gyr (*dashed line*). The solid lines indicate metallicity slopes at the solar radius. Sa ( $d\log(Z)/dr = -0.055 \text{ dex kpc}^{-1}$ ), Sb ( $d\log(Z)/dr = -0.06 \text{ dex kpc}^{-1}$ ), Sc ( $d\log(Z)/dr = -0.065 \text{ dex kpc}^{-1}$ ), Sd ( $d\log(Z)/dr = -0.1 \text{ dex kpc}^{-1}$ ) and Sm ( $d\log(Z)/dr = -0.11 \text{ dex kpc}^{-1}$ ).

duration of the gas infall history are found to be the controlling parameters is in qualitative agreement with standard  $\Lambda$ CDM cosmology which predicts that protodisks reside in dark halos with masses  $\sim 10^{12} M_{\odot}$  and are in a phase of strong gas accretion with values  $>100 M_{\odot}/\text{yr}$  (Burkert & Lin (2006)).

The mass assembly of galaxies occurs through two main processes: hierarchical merging of smaller entities, and more

diffuse gas accretion. The relative importance of the two processes cannot be easily found by cosmological simulations, since many physical parameters such as gas dissipation, star formation and feedback, are still unknown.

There are at least some twenty examples of galaxies which in HI show either signs of interactions and/or have small companions (Sancisi (1999)). This suggests that galaxies often are in an environment where material for ac-

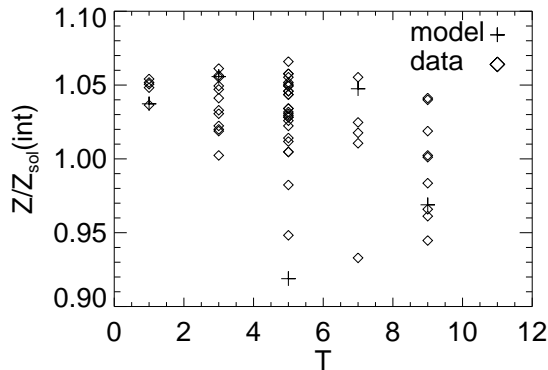


**Figure 12.** The integrated metallicity is plotted versus morphological type. Observational data (*diamond points*) come from Kewley et al. 2005, *plus points* correspond to the improved model predictions.

cretion is available. Characteristic examples are the companions NGC 4565-4565A (Rupen (1991)) and NGC 4027-4027A (Phookun et al. (1992)). These companions have systematic velocities close to those of the main galaxy and HI masses less than 10% of the main galaxy. The HI picture suggests the capture of a gas rich dwarf by a massive system probably to be followed by tidal disruption and accretion of the dwarf. Such examples have been seen also in the Milky Way. The discovery of the Sagittarius dwarf galaxy (Ibata et al. (1994)) shows that accretion is still taking place at the present time.

The model presented here predicts that metal-rich winds are needed especially for Sa type galaxies in order to produce reasonable values for the metallicity today. This prediction is in agreement with suggestions presented in Dalcanton (2006) (for more detailed comments see Section 3.2).

The major shortcoming of the present model is the failure of the chemical enrichment model to reproduce the observed values for nuclear metallicities. Our model predicts very high values for metallicities close to the disk centre for Sa and Sb galaxies whereas the predicted nuclear metallicities for Sd and Sm galaxies are quite low. This is probably due to the high star formation rates that the model predicts in the first  $10^8$  yr, due to our implicit assumption that the entire gas disk has formed instantaneously at  $t = 0$ . The extremely high initial star formation rate result in highly enriched central regions, so enriched that the fresh low metallicity accreted gas cannot dilute the gas efficiently. This is the case especially in galaxies like Sa and Sb characterised by small infall rates. In galaxy types like Sd and Sm, the very high infall rates in the central regions (due to the functional form we assume for the infall model: see Sec 2.6), are enough to dilute metals and result in low values for nuclear metallicities. However the chemical evolution model is in good agreement with observations in terms of the integrated metallicities.

In a future paper, we will develop this model further. Along with the improvements mentioned above, we intend to examine the effect of AGN feedback and compare with numerical simulations.

## REFERENCES

- Abadi G., M., Navarro J. F., Steinmetz M., Eke R., E., ApJ, 2003, 597, 21
- Bower R. G., Benson A. J, Malbon R., Helly J. C., Frenk C. S., Baugh C. M., Cole S., Lacey C. G., 2006, MNRAS, 370, 645
- Bregman J. N., 1980, ApJ, 236, 577
- Burkert A., Lin D. N. C., 2006, preprint
- Chang R., Shu C., Hou J., 2002, Chin. J. Astron. Astrophys., Vol. 2, No 3, 226
- Chiappini C., Matteucci F., Romano D., 2001, ApJ, 554, 1044
- Croton D. J., et al. 2006, MNRAS, 365, 11
- Dalcanton J., J., preprint, astro-ph/0608590
- Dame T. M., 1993, in Holt S. S., Verter F., eds, AIP Conf. Proc. 278, Back to the Galaxy, American Institute of Physics, New York, p.267
- Deul E. R., den Hartog R. H., 1990, A & A, 229, 362
- Dekel A., Silk J., 1986, ApJ, 303, 39
- Efstathiou G., 2000, MNRAS, 317, 697
- Ferreras I., Silk J., 2001, ApJ, 557, 16
- Forster Schreiber N. M. et al., 2006, ApJ, 645, 1062
- Freeman K. C., 1970, ApJ, 160, 811
- Gould A., Bahcall J. N., Flynn C., 1996, ApJ, 465, 759
- Governato F., Willman B., Mayer L., Brooks A., Stinson G., Valenzuela O., Wadsley J., Quinn T., preprint, astro-ph/0602351
- Holmberg J., Flynn C., 2004, MNRAS, 352, 440
- Ibata R. A., Gilmore G., Irwin, 1994, Nature, 370, 194
- Kamphuis J., Sancisi R., 1993, A & A, 273, L31
- Kennicutt R. C., Tamblyn P., Congdon C. W., 1994, ApJ, 435, 22
- Kewley L. J., Jansen R. A., Geller M. J., preprint, astro-ph/0501229
- Klypin A., Zhao H., Somerville S., 2002, ApJ, 573, 597
- MacArthur L. A., Courteau S., Holtzman J. A., 2003, ApJ, 582, 68
- Marquez I., Masegosa J., Moles M., Varela J., Bettoni D., Galletta G., 2002, A & A, 393, 389
- Matteucci F., preprint, astro-ph/0607504
- Naab T., Ostriker J. P., 2006, MNRAS, 366, 899
- Navarro J. F., Frenk C. S., White S. D. M., 1995, MNRAS, 275, 56
- Olling R. P., Merrifield M. R., 2001, MNRAS, 326, 164
- Pagel B., E. 1997, Nucleosynthesis and Chemical Evolution of Galaxies. Cambridge Univ. Press, Cambridge
- Pedersen K. et al. 2006
- Phookun B., Mundy L. G., Teuben P. J., Wainscoat R. J., 1992, ApJ, 400, 516
- Pilyugin L., S., Ferrini F., Shkvarun R. V., 2003, A & A, 401, 557
- Pilyugin L., S., Vilchez J. M., Contini T., 2004, A & A, 425, 849
- Robertson E., Yoshida N., Springel V., Hernquist L., 2004, AJ, 606, 32
- Ricotti M., Ferrara A., 2002, MNRAS, 334, 684
- Rupen M., 1991, AJ, 102, 48
- Sackett P. D., 1997, ApJ, 483, 103
- Sancisi R., 1999, Ap & SS, 269, 59
- Shapiro P. R., Field G. B., 1976, ApJ, 205, 762
- Sharma S., Steinmetz M., 2005, ApJ, 628, 21
- Silk J., MNRAS, 2001, 324, 313
- Silk J., MNRAS, 2003, 343, 249
- Talbot R. J., Arnett W. D., 1975, ApJ, 197, 551
- Strickland D. 2007, MNRAS in press, astro-ph/0701630
- Toomre A., 1964, ApJ, 139, 1217
- Vila-Costas M. B., Edmunds M. G., 1992, MNRAS, 259, 121
- Wang B., Silk J., 1994, ApJ, 427, 759
- Zheng Z., Flynn C., Gould A., Bahcall J. N., Salim S., 2001, ApJ, 555, 393